

# Residential Peak Load Reduction via Direct Load Control under Limited Information

Katharina Kaiser, *Member, IEEE*, Gustavo Valverde, *Senior Member, IEEE*, Gabriela Hug, *Senior Member, IEEE*

**Abstract**—Thermostatically controlled loads and electric vehicles offer flexibility to reduce power peaks in low-voltage distribution networks. This flexibility can be maximized if the devices are coordinated centrally, given some level of information about the controlled devices. In this paper, we propose novel optimization-based control schemes with prediction capabilities that utilize limited information from heat pumps, electric water heaters, and electric vehicles. The objective is to flatten the total load curve seen by the distribution transformer by restricting the times at which the available flexible loads are allowed to operate, subject to the flexibility constraints of the loads to preserve customers' comfort. The original scheme was tested in a real-world setup, considering both winter and summer days. The pilot results confirmed the technical feasibility but also informed the design of an improved version of the controller. Computer simulations using the adjusted controller show that, compared to the original formulation, the improved scheme achieves greater peak reductions in summer. Additionally, comparisons were made with an ideal controller, which assumes perfect knowledge of the inflexible load profile, the models of the controlled devices, the hot water and space heating demand, and future electric vehicle charging sessions. The proposed scheme with limited information achieves almost half of the potential average daily peak reduction that the ideal controller with perfect knowledge would achieve.

**Index Terms**—Direct load control, electric vehicles, electric water heaters, field study, flexible loads, heat pumps, load shifting, peak shaving, residential demand response.

## I. INTRODUCTION

THE electrification of transport and heating in the residential sector, through the adoption of electric vehicles (EVs) and heat pumps (HPs), is a key driver for the energy transition [1]. This electrification poses significant challenges to the operation of distribution grids, including increased load peaks, temporary equipment overloading, and potential voltage issues [2]. At the same time, the rapid adoption of rooftop photovoltaic (PV) systems causes new injection peaks, leading to reverse power flows, overloadings, and voltage rises [3].

As the heating and transportation sectors exhibit considerable flexibility [4], demand-side management in the form of direct control of flexible loads has emerged as a promising strategy to address these challenges [5]. Heating systems can utilize thermal inertia to shift demand [6], and EVs offer great flexibility during the charging process [7]. Direct load control (DLC) can help avoid power peaks in the low-voltage grid and ease the integration of PV systems. Ripple control has been used to disconnect thermostatically controlled loads (TCLs) at

This work is part of a project that received funding from the Swiss Federal Office of Energy (SFOE) under grant number SI/502271.

Katharina Kaiser, Gustavo Valverde, and Gabriela Hug are with the Department of Information Technology and Electrical Engineering, ETH Zurich, 8092 Zurich, Switzerland (e-mail: kkaiser@ethz.ch; gustavov@ethz.ch; ghug@ethz.ch).

specific hours through frequency-ripple signals sent via power cables [8]. However, demand synchronization after the ripple period may result in undesired load rebounds, highlighting the need for new schemes that can distribute demand more evenly throughout the day. Reference [9] provides a comprehensive survey of DLC schemes, organized by control objectives, constraints, methods, and appliances – mainly laundry appliances, TCLs, and EVs. We focus on the latter two for load flattening and peak reductions.

Previous works have proposed direct control of HPs for temporary load reduction [10], [11], the control of EVs for load flattening [12], the use of air conditioners (AC) loads to compensate fluctuations in PV power [13], and load scheduling [14], [15]. However, these algorithms require model training or information that is difficult to monitor, collect, and transmit to a central processor. In [16], the authors proposed predictive control of PVs, EVs, and HPs in the same household to reduce electricity bills, instead of part of a central DLC. Control schemes with prediction capabilities were also reported in [17] and [18] for load shifting of electric water heaters (EWHs), but they rely on information about devices' temperatures or water consumption.

An optimization-based DLC with limited information was proposed in [19] for peak shaving using EWHs. Water temperatures were estimated using hot-water consumption patterns and tank characteristics. However, the estimation errors accumulate over time, which may affect controller performance.

The work in [20] tested a ripple-like DLC scheme to switch off TCLs and EVs according to specific thresholds. The controller was validated in a real-world setup involving five houses and then tested in a simulation environment with 70 houses. However, the controller lacked prediction capabilities.

A few pilot projects have evaluated the response of TCLs to DLC commands in real-world conditions [21]–[23]. These commands were not optimized to flatten the load curve, but to reduce the demand during specific intervals for potential ancillary services. Other field tests have been conducted under controlled environments and simulated water consumption patterns of EWHs [24], [25]. These pilots did not assess peak demand reductions, but focused on the implications for the enrolled customers and information-exchange testing.

Previous DLCs involve mainly homogeneous devices, but the coordination of HPs with EWHs and EVs is expected to maximize their flexibility [26]. Although a limited number of DLCs possess prediction capabilities, they fail to explicitly account for past commands in their current and future decision-making processes. Additionally, most DLCs require measurements or estimations of water and room temperatures, which may be unavailable or difficult to obtain in real

implementations [27]. Finally, the majority of the proposed formulations lack verification in real-world conditions, hiding potential implementation issues and depriving the formulation of improvements where needed.

This paper proposes two DLCs designed to reduce PV injection and demand peaks in low-voltage networks. The schemes optimize the blocking of HPs, EWHs, and EVs in a 24-hour rolling horizon, requiring only limited knowledge of their operating conditions, reflected in flexibility constraints. This approach avoids the need for temperature sensors or detailed TCL thermal models. Moreover, the proposed schemes take into account past commands and predictions of the inflexible load over the next 24 hours. The first version of the controller was implemented in a real-world setup, specifically in a pilot project that controlled tens of devices in a small community in the canton of Zurich. This pilot was part of OrtsNetz, a project carried out by ETH Zurich in collaboration with the Utility of the Canton of Zurich (EKZ). The pilot results showed technical feasibility, but also revealed the need for a refined optimization formulation. The improved scheme addressed the identified drawbacks and was tested in a simulation environment similar to that of the pilot project. Hence, the contributions of this paper are:

- Derivation of new centralized control schemes (L1) and (L2) of residential HPs, EWHs, and EVs to reduce peak loads using limited information. These formulations take into account the flexibility constraints of the controlled devices to guarantee end-user comfort.
- Implementation and performance evaluation of formulation (L1) in a pilot project with 33 TCLs from 22 houses and up to two simultaneous EV charging sessions. Incorporation of the lessons learned from the real-world setup in the refined formulation (L2).
- Impact assessment of the controllers' performance for different information availability conditions. The performance is compared to an ideal setup with perfect knowledge.

The remainder of this paper is organized as follows: Section II presents the proposed DLC formulations with perfect and limited information. Section III describes the setup of the pilot project and the performance of (L1) in the real-world implementation. It also presents a comparison of the different DLC formulations in a simulation environment with conditions similar to those in the real-world setup. The results are further discussed in Section IV, and concluding remarks are presented in Section V.

## II. DLC FORMULATIONS

This section presents DLC formulations with perfect knowledge and with limited information. The proposed DLCs are centralized, optimization-based schemes that aim to reduce power peaks at the transformer station (TS). Given that a flatter load curve generally also leads to improved grid voltage behavior [12] and prevents equipment overloading, grid voltages and currents were not monitored or incorporated into the formulations. For compatibility with different HP and EWH models, the DLCs can only block, but not start, device operation, while EV charging can be started and stopped.

The controller uses a rolling horizon. At each iteration, it considers time steps  $\mathcal{T} = \{0, \dots, T-1\}$  and computes the switching commands for the flexible loads of each customer  $c$ , but only the first  $\kappa$  commands are applied. Device constraints apply to all customers with a given device, though the expression  $\forall c \in \cdot$  is omitted in the formulation for simplicity. Power and energy values are in kW and kWh, respectively, and each time step has a duration of  $\Delta t$  hours.

### A. DLC with perfect knowledge

This subsection introduces the formulation for the ideal DLC which fulfills the same flexibility constraints as the DLC with limited information but assumes perfect knowledge of the HP and EWH models, connection times and charging needs of future EV charging sessions, and the level of inflexible load. This formulation serves as a benchmark for the proposed DLCs with limited information.

1) *HP constraints*: The flexibility constraints are derived from the standard time-based ripple control scheme to ensure customer comfort. In this scheme, HPs can be blocked for up to  $K_{c,HP}^{\text{block},24h}$  time steps per 24-hour window:

$$\sum_{i=t-K+1}^t u_{c,i}^{\text{HP}} \geq K - K_{c,HP}^{\text{block},24h}, \quad \forall t \in \mathcal{T} \quad (1)$$

where  $K$  is the number of time steps in 24 hours ( $24/\Delta t$ ). The binary variables  $u_{c,t}^{\text{HP}}$  denote switching commands. For  $t < 0$ , these are inputs to the optimization. When  $u_{c,t}^{\text{HP}}$  is 0, the HP is blocked and cannot operate. When it is 1, the device may operate or not, depending on the internal device controller. Additionally, HPs can only be blocked for up to  $K_{c,HP}^{\text{max,b}}$  consecutive time steps, and there must be at least  $K_{c,HP}^{\text{min,u}}$  time steps between two blocking instances:

$$\sum_{i=t}^{t+K_{c,HP}^{\text{max,b}}} u_{c,i}^{\text{HP}} \geq w_{c,t}^{\text{HP}}, \quad \forall t \in \{-K_{c,HP}^{\text{max,b}}, \dots, T-1-K_{c,HP}^{\text{max,b}}\} \quad (2)$$

$$\sum_{i=t-K_{c,HP}^{\text{min,u}}+1}^t v_{c,i}^{\text{HP}} \leq u_{c,t}^{\text{HP}}, \quad \forall t \in \mathcal{T} \quad (3)$$

$$w_{c,t}^{\text{HP}} - u_{c,t-1}^{\text{HP}} = v_{c,t}^{\text{HP}} - w_{c,t}^{\text{HP}}, \quad \forall t \in \mathcal{T} \quad (4)$$

The binary variables  $v_{c,t}^{\text{HP}}$  and  $w_{c,t}^{\text{HP}}$  indicate a change in the blocking state and take the value 1 at the start of an unblocked and blocked period, respectively. Introducing these additional variables for formulating minimum/maximum up/down times is preferred to formulating the constraints in the  $u$ -space only, even though it increases the number of binary variables [28]. Finally, a minimum blocking duration of  $K_{c,HP}^{\text{min,b}}$  time steps is specified:

$$\sum_{i=t-K_{c,HP}^{\text{min,b}}+1}^t w_{c,i}^{\text{HP}} \leq 1 - u_{c,t}^{\text{HP}}, \quad \forall t \in \mathcal{T} \quad (5)$$

$$\sum_{i=t-K+K_{c,HP}^{\text{min,b}}}^{t-1} u_{c,i}^{\text{HP}} \geq (K - K_{c,HP}^{\text{block},24h}) \cdot w_{c,t}^{\text{HP}}, \quad \forall t \in \mathcal{T} \quad (6)$$

Besides the flexibility constraints (1) – (6), the HP constraints in the ideal case also include the underlying HP models used in the simulation environment. Both on-off HPs and modulating HPs are modeled with a thermal storage tank. The temperature evolution in the water tank is described by:

$$T_{c,t}^{\text{HP}} = T_{c,t-1}^{\text{HP}} + \frac{P_{c,t}^{\text{HP}} \eta_{c,t}^{\text{HP}} \Delta t - E_{c,t}^{\text{HP}} - E_{c,t}^{\text{HP,loss}}}{V_c^{\text{HP}} \rho_w c_w \cdot \frac{1}{3.6 \cdot 10^6}}, \quad \forall t \in \mathcal{T} \quad (7)$$

where  $T_{c,t}^{\text{HP}}$  is the storage tank temperature at the end of time step  $t$ . The first term in the numerator is the thermal energy supplied by the HP, where  $P_{c,t}^{\text{HP}}$  is the electrical HP power, and  $\eta_{c,t}^{\text{HP}}$  is the HP's coefficient of performance. The parameter  $E_{c,t}^{\text{HP}}$  is the thermal energy withdrawn for space heating, and  $E_{c,t}^{\text{HP,loss}} = \lambda_c^{\text{HP}} (T_{c,t-1}^{\text{HP}} - T_c^{\text{env}}) \Delta t$  are the heat losses, where  $\lambda_c^{\text{HP}}$  is the thermal conductance in  $\text{kW K}^{-1}$  and  $T_c^{\text{env}}$  is the room temperature around the tank.  $V_c^{\text{HP}}$  is the tank size in  $\text{m}^3$ ,  $\rho_w = 1000 \text{ kg m}^{-3}$  is the water density,  $c_w = 4184 \text{ J kg}^{-1} \text{ K}^{-1}$  is the specific heat capacity, and the fraction  $1/(3.6 \cdot 10^6)$  converts Ws to kWh.

The HP power is subject to the operating state  $\rho_{c,t}^{\text{HP}}$ , which depends on the internal hysteresis controller, and the external blocking signal:

$$\rho_{c,t}^{\text{HP}} - \rho_{c,t-1}^{\text{HP}} \leq \frac{T_{c,t}^{\text{HP,LO}} - T_{c,t-1}^{\text{HP}}}{M_1} + 1, \quad \forall t \in \mathcal{T} \quad (8)$$

$$\rho_{c,t}^{\text{HP}} - \rho_{c,t-1}^{\text{HP}} \geq \frac{T_{c,t}^{\text{HP,UP}} - T_{c,t-1}^{\text{HP}}}{M_2} - 1 + u_{c,t}^{\text{HP}} - 1, \quad \forall t \in \mathcal{T} \quad (9)$$

$$\rho_{c,t}^{\text{HP}} \geq \frac{T_{c,t}^{\text{HP,LO}} - T_{c,t-1}^{\text{HP}}}{M_3} + u_{c,t}^{\text{HP}} - 1, \quad \forall t \in \mathcal{T} \quad (10)$$

$$\rho_{c,t}^{\text{HP}} \leq \frac{T_{c,t}^{\text{HP,UP}} - T_{c,t-1}^{\text{HP}}}{M_4} + 1, \quad \forall t \in \mathcal{T} \quad (11)$$

$$\rho_{c,t}^{\text{HP}} \leq u_{c,t}^{\text{HP}}, \quad \forall t \in \mathcal{T} \quad (12)$$

Constraints (8) – (11) without the term  $u_{c,t}^{\text{HP}} - 1$  in (9) and (10) model the hysteresis control. Constraints (8) and (9) keep the operating state unchanged when the temperature is between the lower and upper temperature limits ( $T_{c,t}^{\text{HP,LO}}$  and  $T_{c,t}^{\text{HP,UP}}$ ), while (10) and (11) turn it on (resp. off) when the temperature is below (resp. above) the hysteresis band. The constants  $M_1$  –  $M_4$  must be greater than the expected maximum temperature differences, such that the absolute values of the fractions in (8) – (11) are  $\leq 1$ . The DLC can overrule the HP hysteresis control by blocking device operation. When  $u_{c,t}^{\text{HP}} = 0$ , constraint (12) forces the HP to be off independently of the temperature. To ensure the feasibility of the other constraints during a blocking event, the term  $u_{c,t}^{\text{HP}} - 1$  in (9) and (10) enables turning off even though the temperature is within the specified limits and being off even though the temperature is below the lower limit. After a blocking event, the HP remains off until the temperature drops below the lower bound.

For on-off HPs, the power in time step  $t$  is assumed to be either 0 or the nominal  $P_{c,\text{nom}}^{\text{HP}}$ , depending on the binary variable  $\rho_{c,t}^{\text{HP}}$ , i.e.,

$$P_{c,t}^{\text{HP}} = \rho_{c,t}^{\text{HP}} \cdot P_{c,\text{nom}}^{\text{HP}}, \quad \forall t \in \mathcal{T} \quad (13)$$

Modulating HPs are assumed to match the sum of the thermal demand, the losses, and the energy required to keep the temperature at the lower temperature bound, described by auxiliary variables  $E_{c,t}^{\text{HP,LO}}$ . The resulting power  $\hat{P}_{c,t}^{\text{HP}}$  then needs to be mapped to the feasible power range  $[P_{c,\text{min}}^{\text{HP}}, P_{c,\text{nom}}^{\text{HP}}]$  of the HP. The following constraints reflect this behavior:

$$E_{c,t}^{\text{HP,LO}} = \max \left( 0, \left( T_{c,t}^{\text{HP,LO}} - T_{c,t-1}^{\text{HP}} \right) \cdot \frac{V_c^{\text{HP}} \rho_w c_w}{3.6 \cdot 10^6} \right), \quad \forall t \in \mathcal{T} \quad (14)$$

$$\hat{P}_{c,t}^{\text{HP}} = \frac{E_{c,t}^{\text{HP}} + E_{c,t}^{\text{HP,loss}} + E_{c,t}^{\text{HP,LO}}}{\eta_{c,t}^{\text{HP}} \cdot \Delta t}, \quad \forall t \in \mathcal{T} \quad (15)$$

$$P_{c,t}^{\text{HP}} = \rho_{c,t}^{\text{HP}} \cdot \max \left( P_{c,\text{min}}^{\text{HP}}, \min \left( P_{c,\text{nom}}^{\text{HP}}, \hat{P}_{c,t}^{\text{HP}} \right) \right), \quad \forall t \in \mathcal{T} \quad (16)$$

2) *EWH constraints*: Similar to HPs, EWHs can be blocked for up to  $K_{c,\text{EWH}}^{\text{block,24h}}$  time steps per 24-hour window:

$$\sum_{i=t-K+1}^t u_{c,i}^{\text{EWH}} \geq K - K_{c,\text{EWH}}^{\text{block,24h}}, \quad \forall t \in \mathcal{T} \quad (17)$$

The EWH model in the ideal DLC is the same as the model for on-off HPs, except that (i) the coefficient of performance is assumed to be 1 and is therefore discarded, and (ii) the temperature limits are time-independent for EWHs. Hence, the constraints include (17) and (7) – (13) adapted to EWHs.

3) *EV constraints*: The ideal DLC takes into account all controllable charging sessions  $\mathcal{S}_c = \{0, \dots, S_c\}$  of each customer  $c$  in the optimization horizon. The first time step of each session  $s$  is denoted as  $t_{c,s}^{\text{EV,a}}$ . It corresponds to the start time of a future charging session or time step 0 if the session is ongoing. Additionally, the customer specifies the departure time step  $t_{c,s}^{\text{EV,d}}$  and the corresponding desired state-of-charge  $\text{SoC}_{c,s}^{\text{EV,goal}}$  for each controllable charging session. Given the SoC at the end of time step  $t_{c,s}^{\text{EV,a}} - 1$ , the desired SoC, the charging efficiency  $\eta_c^{\text{EV}}$ , the nominal charging power  $P_{c,\text{nom}}^{\text{EV}}$ , and the battery capacity  $E_c^{\text{EV}}$ , the number of time steps for which the EV needs to charge until departure is:

$$N_{c,s}^{\text{EV,goal}} = \left\lceil \left( \text{SoC}_{c,s}^{\text{EV,goal}} - \text{SoC}_{c,t_{c,s}^{\text{EV,a}}-1}^{\text{EV}} \right) \cdot \frac{E_c^{\text{EV}}}{P_{c,\text{nom}}^{\text{EV}} \cdot \eta_c^{\text{EV}} \cdot \Delta t} \right\rceil \quad (18)$$

and the number of charging time steps to reach a given minimum SoC is:

$$\hat{N}_{c,s}^{\text{EV,min}} = \left\lceil \left( \text{SoC}_c^{\text{EV,min}} - \text{SoC}_{c,t_{c,s}^{\text{EV,a}}-1}^{\text{EV}} \right) \cdot \frac{E_c^{\text{EV}}}{P_{c,\text{nom}}^{\text{EV}} \cdot \eta_c^{\text{EV}} \cdot \Delta t} \right\rceil \quad (19)$$

In case the desired SoC is smaller than the minimum SoC, charging should be stopped after reaching the desired SoC, with  $N_{c,s}^{\text{EV,min}} = \min(\hat{N}_{c,s}^{\text{EV,min}}, N_{c,s}^{\text{EV,goal}})$ . These values are used in the following constraints to enforce that (i) the EV reaches the desired SoC at departure, and (ii) charging is only stopped after

reaching the minimum SoC, which is introduced to reduce customers' dissatisfaction in case of communication issues:

$$\sum_{i=t_{c,s}^{\text{EV,a}}}^{t_{c,s}^{\text{EV,d}}-1} u_{c,i}^{\text{EV}} = N_{c,s}^{\text{EV,goal}}, \quad \forall s \in \mathcal{S}_c \text{ with } t_{c,s}^{\text{EV,d}} \leq T \quad (20)$$

$$\sum_{i=t_{c,s}^{\text{EV,a}}}^{T-1} u_{c,i}^{\text{EV}} \leq N_{c,s}^{\text{EV,goal}}, \quad \forall s \in \mathcal{S}_c \text{ with } t_{c,s}^{\text{EV,d}} > T \quad (21)$$

$$\sum_{i=t_{c,s}^{\text{EV,a}}}^{t_{c,s}^{\text{EV,a}}+N_{c,s}^{\text{EV,min}}-1} (1 - u_{c,i}^{\text{EV}}) = 0, \quad \forall s \in \mathcal{S}_c \text{ with } t_{c,s}^{\text{EV,a}} + N_{c,s}^{\text{EV,min}} \leq T \quad (22)$$

$$\sum_{i=t_{c,s}^{\text{EV,a}}}^{T-1} (1 - u_{c,i}^{\text{EV}}) = 0, \quad \forall s \in \mathcal{S}_c \text{ with } t_{c,s}^{\text{EV,a}} + N_{c,s}^{\text{EV,min}} > T \quad (23)$$

$$u_{c,t}^{\text{EV}} \leq \phi_{c,t}^{\text{EV}}, \quad \forall t \in \mathcal{T} \quad (24)$$

The binary parameter  $\phi_{c,t}^{\text{EV}}$  in (24) denotes whether the EV is plugged in, and the binary variable  $u_{c,t}^{\text{EV}}$  denotes whether it charges. Additionally, communication capabilities limit the number of off-to-on switchings in any 24-hour window to  $K_{c,\text{EV}}^{\text{max,24h}}$ :

$$\sum_{i=t-K+1}^t b_{c,i}^{\text{EV}} \leq K_{c,\text{EV}}^{\text{max,24h}}, \quad \forall t \in \mathcal{T} \quad (25)$$

$$b_{c,t}^{\text{EV}} \geq (u_{c,t}^{\text{EV}} - u_{c,t-1}^{\text{EV}}) \cdot \phi_{c,t-1}^{\text{EV}}, \quad \forall t \in \mathcal{T} \quad (26)$$

where the binary variable  $b_{c,t}^{\text{EV}}$  describes an off-to-on transition. Upon arrival, the EV starts charging by default, which is not counted as a start signal. Finally, each EV is assumed to charge with the given nominal power when  $u_{c,t}^{\text{EV}} = 1$ :

$$P_{c,t}^{\text{EV}} = u_{c,t}^{\text{EV}} \cdot P_{c,\text{nom}}^{\text{EV}}, \quad \forall t \in \mathcal{T} \quad (27)$$

Potential average power deviations in the last time step due to the battery being full are neglected.

4) *Objective Function:* The ideal DLC minimizes the highest absolute total power in the optimization horizon:

$$\min P^{\text{max}} \quad (28a)$$

$$\text{s.t. } P_t^{\text{max}} \geq P_t^{\text{tot}}, \quad \forall t \in \mathcal{T} \quad (28b)$$

$$P_t^{\text{max}} \geq -P_t^{\text{tot}}, \quad \forall t \in \mathcal{T} \quad (28c)$$

$$P_t^{\text{tot}} = P_t^{\text{inf}} + \sum_{c \in \mathcal{C}^{\text{HP}}} P_{c,t}^{\text{HP}} + \sum_{c \in \mathcal{C}^{\text{EWH}}} P_{c,t}^{\text{EWH}} + \sum_{c \in \mathcal{C}^{\text{EV}}} P_{c,t}^{\text{EV}}, \quad \forall t \in \mathcal{T} \quad (28d)$$

where  $P_t^{\text{inf}}$  is the inflexible load at TS level, i.e., the load that is not controlled by the DLC, and  $\mathcal{C}^{\text{HP}}$ ,  $\mathcal{C}^{\text{EWH}}$ , and  $\mathcal{C}^{\text{EV}}$  are the sets of customers with a corresponding controllable device.

## B. DLC with limited information

In the given real-world setup, the central controller knows the nominal power values for HPs and EWHs, as well as the EV charging demand during ongoing charging sessions. However, it lacks knowledge of future charging sessions and TCL temperatures, and relies on estimates for the inflexible power  $P_t^{\text{inf}}$  at the TS level, as well as the HP and EWH

demand. Hence, the formulation of the optimization problem needs to be adapted.

1) *HP constraints:* The HP constraints include (1) – (6) for all customers with an HP, and the power is estimated based on the ambient temperature, represented by the parameter  $0 \leq \alpha_t^{\text{HP}} \leq 1$  (cf. Section III-A3):

$$P_{c,t}^{\text{HP}} = u_{c,t}^{\text{HP}} \cdot \alpha_t^{\text{HP}} \cdot P_{c,\text{nom}}^{\text{HP}}, \quad \forall t \in \mathcal{T} \quad (29)$$

2) *EWH constraints:* Two different formulations to model EWH operation are investigated. The optimization problems corresponding to these two formulations are referred to as (L1) and (L2). Constraint (17) applies in both cases.

In (L1), constraints (2) – (6), which specify a minimum and maximum blocking duration and a minimum duration between two blocking instances, are also introduced for EWHs. The inclusion of a minimum blocking duration reduces the uncertainty related to EWHs being on when unblocked because after a long blocking period, implemented by choosing a high value for  $K_{c,\text{EWH}}^{\text{min,b}}$ , an EWH is likely to operate as soon as it is unblocked. The EWH power demand is:

$$P_{c,t}^{\text{EWH}} = u_{c,t}^{\text{EWH}} \cdot P_{c,\text{nom}}^{\text{EWH}}, \quad \forall t \in \mathcal{T} \quad (30)$$

This formulation was tested in the pilot project, as described in Section III-A. An alternative, improved formulation (L2) is tested in Section III-B. It includes additional binary variables  $\rho_{c,t}^{\text{EWH}}$  that model the EWH power demand when the device is unblocked. We assume that the EWH runs during the first  $K_{c,\text{EWH}}^{\text{run}}$  time steps of an unblocking period and demands the nominal power  $P_{c,\text{nom}}^{\text{EWH}}$ . The following constraints enforce  $\rho_{c,t}^{\text{EWH}} = 1$  for the first  $K_{c,\text{EWH}}^{\text{run}}$  time steps of an unblocking period, and 0 otherwise:<sup>1</sup>

$$\rho_{c,t}^{\text{EWH}} \geq \sum_{i=t-K_{c,\text{EWH}}^{\text{run}}+1}^t v_{c,i}^{\text{EWH}}, \quad \forall t \in \mathcal{T} \quad (31)$$

$$\rho_{c,t}^{\text{EWH}} \leq 1 - \sum_{i=t-K_{c,\text{EWH}}^{\text{run}}+1}^{t-K_{c,\text{EWH}}^{\text{run}}} v_{c,i}^{\text{EWH}}, \quad \forall t \in \mathcal{T} \quad (32)$$

$$\rho_{c,t}^{\text{EWH}} \leq u_{c,t}^{\text{EWH}}, \quad \forall t \in \mathcal{T} \quad (33)$$

To model that the EWH may still operate during some of the remaining unblocked time steps, we account for 10 % of the nominal power when  $u_{c,t}^{\text{EWH}} = 1$  and  $\rho_{c,t}^{\text{EWH}} = 0$ :

$$P_{c,t}^{\text{EWH}} = (0.1 \cdot u_{c,t}^{\text{EWH}} + 0.9 \cdot \rho_{c,t}^{\text{EWH}}) \cdot P_{c,\text{nom}}^{\text{EWH}}, \quad \forall t \in \mathcal{T} \quad (34)$$

In contrast to (L1), the constraint set includes only (3) – (6) adapted to EWHs. Furthermore, an upper limit on the number of consecutive unblocked time steps is added:

$$\sum_{i=t}^{t+K_{c,\text{EWH}}^{\text{max,u}}} (1 - u_{c,i}^{\text{EWH}}) \geq v_{c,t}^{\text{EWH}}, \quad \forall t \in \{-K_{c,\text{EWH}}^{\text{max,u}}, \dots, T-1-K_{c,\text{EWH}}^{\text{max,u}}\} \quad (35)$$

<sup>1</sup> An alternative formulation is  $\rho_{c,t}^{\text{EWH}} = \sum_{i=t-K_{c,\text{EWH}}^{\text{run}}+1}^t v_{c,i}^{\text{EWH}}$ ; however, with the studied settings, the given formulation reduced computation time.

TABLE I  
OVERVIEW OF THE AVAILABLE INFORMATION AND THE CONSTRAINTS FOR THE INVESTIGATED CASES.

		Ideal			Limited			Settings			
		L1	L2	L2-PF	$K_{c,\cdot}^{\text{block},24h}$	$K_{c,\cdot}^{\text{min},b}$	$K_{c,\cdot}^{\text{max},b}$	$K_{c,\cdot}^{\text{min},u}$	$K_{c,\text{EWH}}^{\text{max},u}$	$K_{c,\text{EWH}}^{\text{run}}$	$K_{c,\text{EV}}^{\text{max},24h}$
Obj. function		(28)	(36)	(36)	(36)						
HP flexibility	(1) – (6)		✓	✓	✓	✓		16	4	8	8
EWL flexibility	(17)		✓	✓	✓	✓	64 – 78				
HP power, actual model	(7) – (16)		✓								
EWL power, actual model	(7) – (13) for EWHs		✓								
HP power, estimation	(29)			✓	✓	✓					
EWL power, estimation L1	(2) – (6) for EWHs, (30)		✓				19		56 – 72	6 – 8	
EWL power, estimation L2	(3) – (6) for EWHs, (31) – (35)			✓	✓		40		12	40	6
EV charging flexibility	(20) – (26)		✓	✓	✓	✓					
EV charging power	(27)		✓	✓	✓	✓					3
Input	EV charging sessions	only ongoing (o) or all (a)	a	o	o	a					
	Inflexible load profile	estimated (e) or actual (a)	a	e	e	a					

3) *EV constraints*: The DLC with limited information considers an EV's charging demand as soon as a charging session starts and the customer specifies the departure settings. The constraint set includes (24) – (27) and (20) – (23) for ongoing sessions, i.e., those including time step 0. An EV is assumed to be disconnected for  $t \geq t_{c,0}^{\text{EV},d}$  ( $\phi_{c,t}^{\text{EV}} = 0$ ).

4) *Objective function*: To reduce the impact of prediction errors, we not only target the single highest peak in the time horizon, but also aim to flatten the overall load curve by choosing a quadratic objective function. It penalizes deviations of the total power from a specified reference value  $P^{\text{ref}}$ :

$$\min \sum_{t=0}^{T-1} (P_t^{\text{tot}} - P^{\text{ref}})^2 \quad (36a)$$

$$\text{s.t. } P_t^{\text{tot}} = P_t^{\text{inf}} + \sum_{c \in \mathcal{C}^{\text{HP}}} P_{c,t}^{\text{HP}} + \sum_{c \in \mathcal{C}^{\text{EWH}}} P_{c,t}^{\text{EWH}} + \sum_{c \in \mathcal{C}^{\text{EV}}} P_{c,t}^{\text{EV}}, \forall t \in \mathcal{T} \quad (36b)$$

where  $P_t^{\text{inf}}$  are now predictions of the inflexible load at the TS level over the optimization horizon, see Section III-A2.

### C. Variants and settings

Table I summarizes the DLC with perfect and with limited information, and provides the parameter values for the different constraints with  $\Delta t = 0.25$  h. The values for  $K_{c,\text{HP}}^{\text{block},24h}$ ,  $K_{c,\text{HP}}^{\text{max},b}$ ,  $K_{c,\text{HP}}^{\text{min},u}$ , and  $K_{c,\text{EWH}}^{\text{block},24h}$  are based on EKZ's standard ripple control, and the value for  $K_{c,\text{EWH}}^{\text{run}}$  is based on the median average EWH runtime obtained in [29]. SoC<sub>c</sub><sup>EV,min</sup> is set to 0.5 for all cases.

The implementation in the pilot corresponds to (L1) with the minimum/maximum up/down constraints formulated in the  $u$ -space only (cf. Section II-A1), an alternative formulation for the EV constraints (20) and (21), which includes the SoC evolution, and without (6), allowing for potential invalid blockings at the end of the optimization horizon. This variant is referred to as (L1-Pilot), and the detailed formulation is provided in [30]. The simulations evaluate the peak-shaving performance of (Ideal), (L1-Pilot), (L1), (L2), and one intermediate case (L2-PF) with perfect foresight regarding EV charging sessions and the inflexible load, but estimations for the HP and EWH

power demand. The latter is introduced to assess the impact of future charging sessions and the inflexible load estimation.

### III. CASE STUDY

In the following, we first describe the real-world pilot setup and the inflexible load, HP power, and baseline estimation. Subsequently, we present the pilot results and provide further insights based on simulations.

#### A. Pilot

1) *Experimental setup and infrastructure*: For testing the DLC with limited information in a real-world pilot application, load control devices were installed at 22 single-family homes that are connected to the same TS. Unlike the standard ripple control, which blocks groups of loads simultaneously, the new devices allow for individualized commands for each HP and EWH. Every 15 minutes ( $\kappa = 1$ ), the blocking commands for the next 24 hours ( $T = 96$ ) were computed in the central optimization using the Gurobi [31] solver, configured with a 5-minute time limit and the barrier method for solving the root and node relaxations. The resulting commands were communicated to the local devices via power line communication. A local verification module corrected the commands in case they did not satisfy the flexibility constraints (1) – (6) and (17), e.g., due to communication issues. The central system retrieved the actually applied blocking actions and the 15-minute smart meter (SM) measurements once a day. Additionally, several EVs in the same municipality were virtually connected to the TS under study, i.e., their charging profiles were added to the TS load even though they were physically connected to a different TS. EV charging was controlled via an application programming interface (API) that can start and stop charging and retrieve the vehicles' current status. In each iteration of the rolling horizon, the optimization considered the EVs that were available for control at the given moment. For consistency, the analyses also consider only those EV charging sessions captured in at least one optimization window. During the pilot period, the relevant EV customers and all customers connected to the given TS received a unit tariff instead of the existing two-tier tariff [30]. HPs and EWHs without the new control

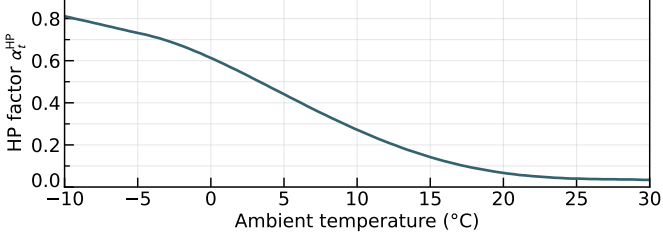


Fig. 1. Estimated variation of the HPs' power demand with ambient temperature.

device remained under the standard ripple control, and were considered part of the inflexible load.

2) *Inflexible load estimation and  $P^{\text{ref}}$* : The DLC needs a 24-hour-ahead prediction of the inflexible load  $P^{\text{inf}}$  at the TS level in (36). To enable such a prediction, past SM data of every house was first disaggregated to create a database of historical flexible (HP and EWH) demand. Later, predicted ambient temperature and global irradiation data were used to identify the day that, out of the historical data, is most similar to the considered day. This day is referred to as most similar day (MSD). Finally, the inflexible load prediction for this day was calculated by subtracting the flexible load profiles (HP, EWH, and EV, the latter through direct measurement) from the total TS load of the MSD.

Preliminary tests found that using  $P^{\text{ref}} > 0$  in formulation (L1-Pilot) would result in flatter total load curves. The value of  $P^{\text{ref}}$  in (36) was set to the average total power at the TS level for the identified MSD.

3) *HP power estimation*: The power demand of each HP is estimated as its nominal power multiplied by the correction parameter  $0 \leq \alpha_t^{\text{HP}} \leq 1$ . This parameter represents the variation of HPs' power demand with ambient temperature. It is computed from a regression model extracted from two years of historical data of the power demand of dozens of HPs in Zurich and the corresponding ambient temperature. Fig. 1 displays the curve that was fitted to four-hour average temperature and power values. The regression model is used to determine  $\alpha_t^{\text{HP}}$  given an ambient temperature forecast. This parameter is assumed to be equal for all devices.

4) *Baseline load estimation*: The TS load profile without the DLC needs to be estimated to evaluate the DLC performance in the pilot. This work follows the baseline load estimation approach described in [32]. The baseline load for a given pilot day is estimated as the actual TS load profile, minus the EV charging load during controlled sessions, plus the load profiles of those sessions with uncontrolled charging, minus the SM profiles of households with an OrtsNetz load control device on the pilot day, plus the SM profiles of those households on the corresponding MSD. Two different MSD matching approaches are considered to strengthen the validity of the findings. The MSD is identified either as (a) the day with the most similar weather conditions — as described above for the inflexible load estimation — or (b) the day whose load profile, considering only non-participants in the pilot municipality, is most similar. The reader is referred to [32] for more details.

TABLE II  
DATES FOR THE PILOT EVALUATION.

Season	OrtsNetz pilot		Baseline period	
	Dates	Scheme	Dates	
Summer	29.08.24 - 04.09.24	Ripple control	01.06.23 - 14.09.23	
Winter	19.11.24 - 19.12.24 19.11.24 - 19.12.24	Ripple control No control	01.01.23 - 31.03.23 20.12.23 - 27.02.24	

5) *Results*: Table II gives the dates for evaluating injection and consumption peak reductions in summer and winter, respectively. During the evaluated pilot periods, 90.1 % (resp. 89.7 %) of the HPs (resp. EWHs) commands used as input by the local control devices matched the signals sent by the central controller. The local verification, which was implemented to filter out invalid DLC commands, changed the HP and EWH commands 7.2 % and 16.5 % of the time, respectively. These changes stem from communication issues and a mismatch between the central and local settings for  $K_{c,\text{EWH}}^{\text{block},24h}$  for some EWHs, which led to additional unblockings of up to 3.5 hours.

The left column of Fig. 2 shows the pilot results for summer. Fig. 2(a) compares the distribution of daily injection peaks in OrtsNetz, i.e., the DLC with formulation (L1-Pilot), and the corresponding baseline load profiles with ripple control, according to the weather and non-participants MSD matching approaches. The DLC reduced the injection peaks by 4 or 5 kW on average, depending on the matching approach. Fig. 2(c) compares the mean daily TS power as a result of OrtsNetz with ripple control, and the corresponding aggregated profiles of SMs, which were replaced to obtain the baseline load estimate. It illustrates that the DLC shifts the EWH operation from nighttime to late morning. Furthermore, it suggests that greater reductions could have been achieved if the EWHs had consumed more power during the peak PV injection hours. As shown in Fig. 2(e2), although most EWHs were unblocked from 9 am to 5 pm, they primarily demanded power in the initial hours after the unblocking signals, i.e., consumed power before the injection peaks. Formulation (L2) addresses this deficiency and is investigated in simulations.

In winter, the baseline periods from which MSDs were selected include days when the ripple control was active and when no control scheme was in effect (see Table II). In the no-control setting, all devices connected to an OrtsNetz control device were unblocked for the entire day and could therefore operate freely according to their internal device controllers. The right column of Fig. 2 presents the evaluation results for winter days. HPs and other heating systems dominate the TS demand. Hence, consumption peaks become the determining factor. Fig. 2(b) shows that the DLC reduced the consumption peaks by an average of 2 to 5 kW with respect to the ripple control. However, no peak reductions were observed compared to no control. The comparison of the SM profiles in Fig. 2(d2) shows that the DLC distributed the flexible demand more evenly throughout the day, with some demand concentration between 9 am and 7 pm. For a more detailed investigation, Fig. 2(f) presents the share of unblocked EWHs and blocked HPs on a single day. At the two consumption peaks of the TS,

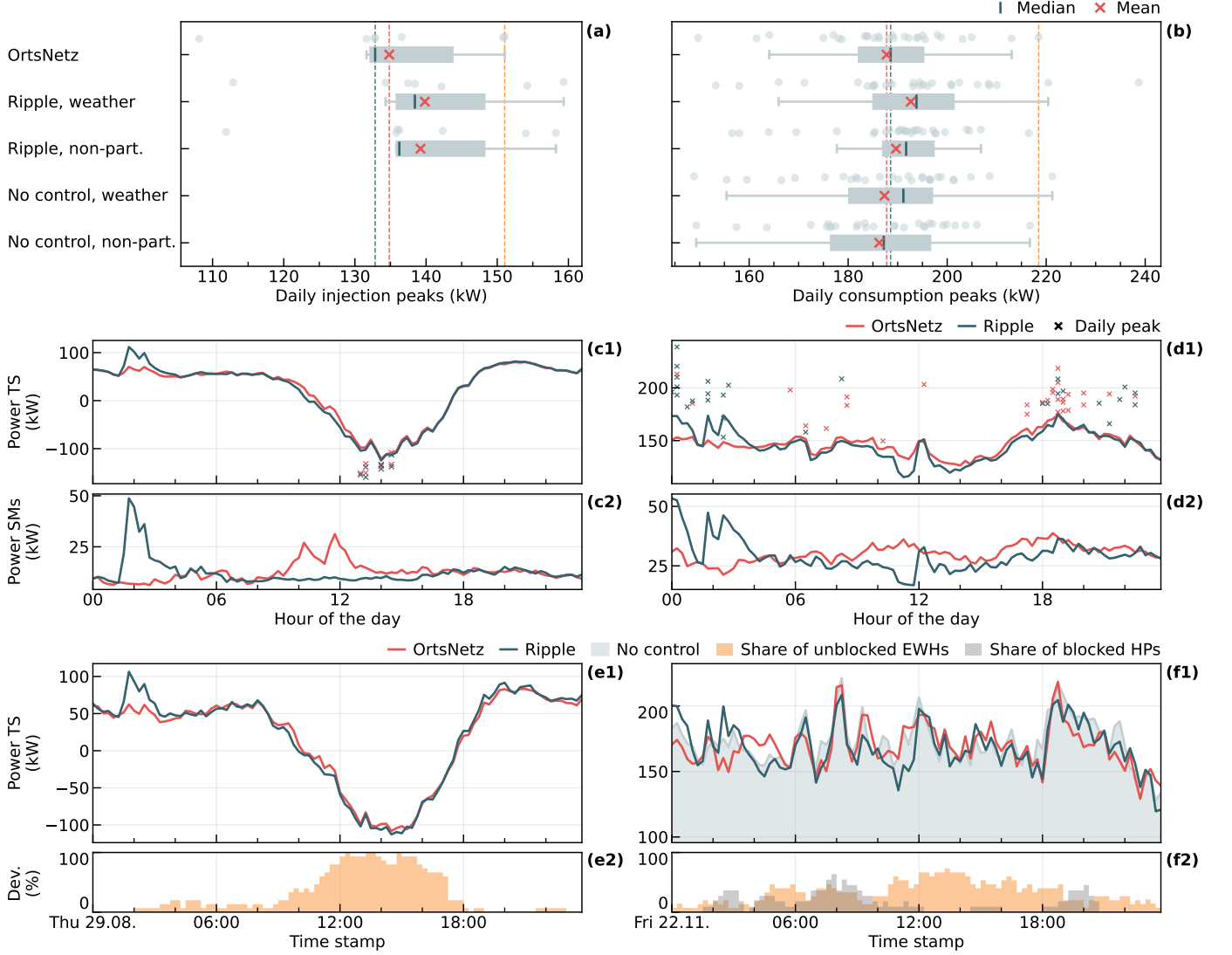


Fig. 2. Pilot results for summer (left) and winter (right): Distribution of daily peaks (top), mean daily profiles and daily peak values using the MSD based on weather data (middle), and TS load profiles and device blockings for a single day using the MSD based on weather data (bottom).

several HPs and EWHs were blocked, yet insufficient to prevent the peaks. As reported in the load profiles comparison of Fig. 2(f1), the DLC reduced the consumption peak experienced in the early hours, but there was no clear advantage when compared to the no-control case for other hours. During the consumption peaks, the DLC reached almost the same demand values as those without control.

In the final project survey, none of the pilot DLC participants reported undesired changes in controlled temperature. This suggests that the proposed constraints provide enough room for the devices' normal operation while providing flexibility when needed. However, three survey responses indicate that future implementations should provide clear explanations of the HP and EWH flexibility constraints to the customers.

### B. Simulations

While the real-world results demonstrate technical feasibility, they may have been affected by the uncertainties in the baseline load estimate and technical issues [32]. The

following simulations eliminate these aspects and investigate the performance of the variants introduced in Section II-C.

1) *Setup*: The simulation environment emulates the TS used to test the DLC in the real-world pilot. The inflexible load profile  $P^{\text{inf}}$  is derived by (i) subtracting the SM profiles of controllable households from the total TS load, (ii) adding the average SM profile of inflexible customers without electric heating, EWH, EV, and PV, scaled by the number of controlled households, and (iii) subtracting the generation profile of two separately measured PV installations, scaled to match the controlled households' PV generation. The parameters for the HP and EWH models (see Section II-A) are derived as described in [33], except that (i) the EWH storage tank volumes are taken from installation data, and (ii) the HP storage tanks are sized to be able to bridge between 1 and 2 hours of blocking at the maximum heat demand, similar to [34]. HPs with a nominal electrical power greater than or equal to 7 kW are modeled as modulating HPs, with  $P_{c,\text{min}}^{\text{HP}} = 0.3 \cdot P_{c,\text{nom}}^{\text{HP}}$ . All other HPs are assumed to be on-

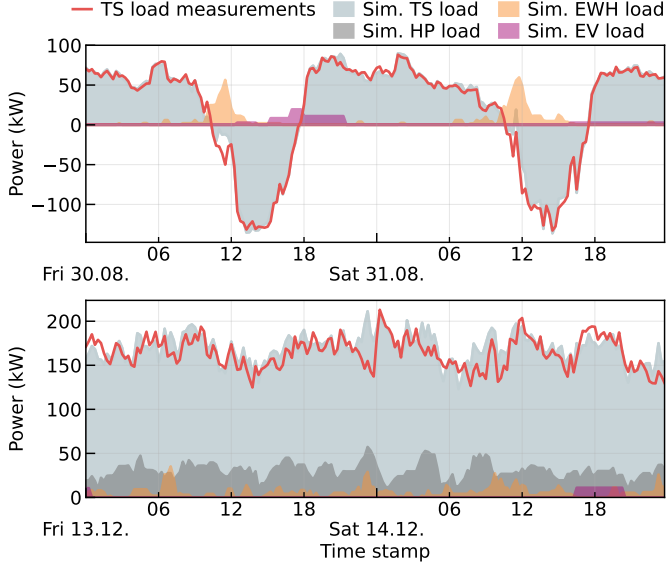


Fig. 3. Measured and simulated load for two summer days (top) and two winter days (bottom).

off-controlled. The EV data and charging characteristics are based on real-world data from the pilot with the additional assumptions that each EV has a fixed charging power and battery capacity, and that the charging efficiency is 90 %. The recorded EV plug-in times, SoC at plug-in, and SoC at departure are used to determine each session's requirements.

Simulations are carried out for two periods: one week in summer (August 29th to September 4th, 2024) and one in winter (December 9th to December 15th, 2024). Devices are initialized by running the simulation without external control for two additional days prior to the start of each period.

As visualized in Fig. 3, the simulated TS load is generally aligned with the real-world measurements. In this comparison, HPs and EWHs were simulated using the blocking commands that were applied during the pilot, and the EV load represents immediate charging.

The computation time limit to solve the optimization problem in the perfect knowledge case is set to 1 hour, and the optimization window is shifted by 6 hours between iterations ( $\kappa = 24$ ). For all other cases, the time limit remains the same as in the pilot, i.e., 5 minutes, and the optimization window is shifted by 1 hour ( $\kappa = 4$ ). For all cases except (L1-Pilot), the solution of the previous iteration is used as a warm start for the next iteration. The estimation for  $P^{\text{inf}}$  and  $P^{\text{ref}}$  are the same as during the pilot for (L1-Pilot), (L1), and (L2). For (L2-PF),  $P^{\text{inf}}$  is equal to the actual inflexible load used in the simulations, and  $P^{\text{ref}}$  is fixed at 0 and 160 kW in summer and winter, respectively.

2) *Results:* Fig. 4 shows the load duration curves for summer and winter. Each curve displays the average power in every 15-minute time step of the evaluation period in descending order. Additionally, Table III summarizes the peak reduction results. The metrics are computed with respect to the simulation with ripple control.  $\overline{\Delta P^{\text{max}}}$  is the average of the peak reductions on the evaluated days, while  $\Delta P^{\text{max}}$  is

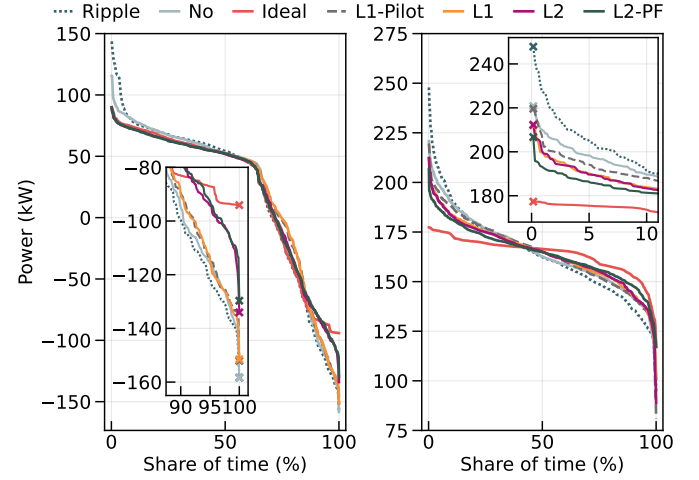


Fig. 4. Duration curves for the simulations in summer (left) and winter (right).

TABLE III  
SIMULATION RESULTS FOR INJECTION AND CONSUMPTION PEAKS IN SUMMER AND WINTER, RESPECTIVELY.

	Scheme	$\overline{\Delta P^{\text{max}}}$ (kW)	$\overline{\Delta P^{\text{max}}}/P^{\text{EWH}}$ (%)	$\Delta P^{\text{max}}$ (kW)
Summer	No control	2.96	3.2	0.00
	L1-Pilot	8.71	9.3	6.25
	L1	7.25	7.8	6.80
	L2	27.47	29.5	24.30
	L2-PF	30.38	32.6	28.66
	Ideal	57.26	61.4	64.27
Winter	No control	10.81	-	27.05
	L1-Pilot	17.57	-	28.26
	L1	22.18 (20.68)	-	35.83
	L2	21.82 (20.32)	-	35.55 (25.05)
	L2-PF	29.88 (27.08)	-	41.17
	Ideal	52.17 (46.40)	-	70.52 (65.75)

the maximum peak reduction, i.e., the difference between the highest values across the entire week with the given scheme and with ripple control. Since in summer, EWHs are the main source of flexibility in the given setup, we additionally present the results for the ratio  $\overline{\Delta P^{\text{max}}}/P^{\text{EWH}}$ , where  $P^{\text{EWH}}$  is the sum of the controlled EWHs' nominal power values. This allows to generalize the results to other system configurations. Finally, values in parentheses show the results with immediate EV charging, i.e., without using the EVs' flexibility. These values are shown if they differ from the simulation with EV flexibility.

These results yield five main observations. First, the no-control results suggest that removing the ripple control may reduce peaks, which is in line with the real-world results (cf. Fig. 2(b)) and the results in [32]. Second, (L1-Pilot) performs similarly to (L1) in summer, and slightly worse than (L1) in winter. Fig. 5 reveals that high mixed-integer programming (MIP) gaps occurred for (L1-Pilot), both in simulations and during the pilot. In addition to the differences described in Section II-C, the implementation for (L1-Pilot) did not use auxiliary variables  $P_t^{\text{tot}}$  in (36). Instead,

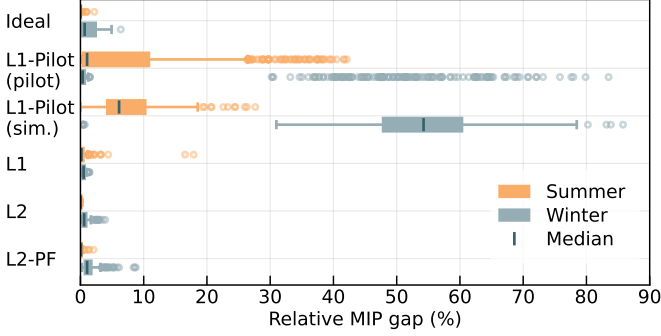


Fig. 5. Relative MIP gap per iteration during the simulated periods.

it included the products in (27), (29), and (30) directly in the objective function. High gaps occurred particularly when the solver linearized the resulting products of binary variables (the parameter `PreQLinearize` was at its default setting, i.e., automatic choice). Introducing the variables  $P_t^{\text{tot}}$ ,  $v_{c,t}$ ,  $w_{c,t}$ , and warm-starting the optimization reduces the gaps in the other cases. Third, (L2) leads to higher injection peak reductions than (L1) due to the better representation of the EWH operation when unblocked. Fig. 6(a) illustrates that, contrary to (L1), (L2) concentrates EWH demand at the hours of maximum PV injection. Fourth, the performance of (L2-PF) with perfect foresight of EV charging sessions and the inflexible load is comparable to (L2) in summer, but achieves further reductions in consumption peaks in winter. This is also illustrated in Fig. 6(b). Finally, the recommended formulation with limited information, (L2), could realize 48.0 % and 41.8 % of the potential average daily peak reduction  $\overline{\Delta P^{\text{max}}}$  with (Ideal) in summer and winter, respectively.

#### IV. DISCUSSION

The simulation results demonstrate that the proposed DLC schemes with limited information reduce injection and consumption peaks at a TS level, and that the formulation (L2) addresses the deficiency of (L1) in modeling the EWH power demand. Additionally, the real-world results demonstrate that the approach is technically feasible and preserves customer comfort, enabling utilities to leverage the flexibility of major loads for peak reduction with only a few changes to the existing infrastructure. However, there are some limitations that are discussed in the following and may be addressed in future work. We focus on the formulation with limited information, which is the most relevant for practical application. First, the comparison between (L2) and (L2-PF) shows that improving the inflexible load estimates could enhance performance. Second, the HP power estimation may be improved. Fig. 7 compares the optimization and simulation results for the formulation (L2-PF) on two winter days. The results deviate because (L2-PF) uses EWH and HP power estimations (cf. Table I), whereas the simulation environment, to which the resulting switching commands are applied, uses the more detailed models that were introduced as part of the ideal formulation (cf. Section II-A). The figure shows that the EWH power demand in the simulations aligns with the estimates in

the optimization, whereas there are significant differences for the HP power. Future work could refine the HP power estimation and model power rebounds after blocking periods [22]. Third, the flexible EV charging load is low in the given case study (on average 10 and 20.5 kWh per day in the summer and winter simulation, respectively). It is expected that a larger fleet of controllable EVs will make the benefits of a DLC even more evident. At the same time, forecasting future sessions may become necessary for larger EV fleets. Finally, further investigations showed that the quadratic objective function (36) may yield flexible load reductions at off-peak times when the total flexible energy in the optimization horizon is not fixed. This applies to the HP power estimation, which is a function of the temperature-dependent HP parameter  $\alpha_t^{\text{HP}}$ . In this case, the objective function value may be smaller when reducing overall consumption rather than reducing the flexible load at times when the inflexible load is high. The choice of  $P^{\text{ref}}$  impacts this trade-off. Furthermore, note that even if the total energy is fixed, the quadratic objective function may not yield the smallest peak value (consider, e.g., three time steps with total power (6, 3, 2) compared to (5, 5, 1), with  $P^{\text{ref}} = 0$ ).

#### V. CONCLUSION

The proposed DLCs with limited information (L1 and L2) determine the times when the available flexible loads should be unblocked to flatten the total 24-hour load curve. They use a prediction of the inflexible load, obtained from historical data, and the flexibility constraints of HPs, EWHs, and EVs. The pilot DLC demonstrated that, in summer, the unblocked EWHs experienced early consumption, i.e., immediately after being unblocked, which prevented the DLC (L1) from reducing the highest injection peaks; this issue was addressed in formulation (L2). In winter, the pilot DLC spread the flexible load throughout the day, resulting in larger consumption peak reductions compared to ripple control, but comparable to those without control. Simulation results showed that the improved formulation (L2) yields greater injection peak reductions than (L1), due to a more accurate representation of the EWH operation when unblocked. Finally, it was found that (L2), with limited information, could achieve 48.0 % and 41.8 % of the potential average daily peak reduction with perfect knowledge in summer and winter, respectively.

#### ACKNOWLEDGMENTS

We thank Marina González Vayá and Ludger Leenders from EKZ for enabling the real-world implementation, and Markus Kreft and Thorsten Staake from ETH Zurich for valuable discussions and their support. We also gratefully acknowledge the contributions of Matteo Gussetti, Hendrik Lohse, Federico Lo Curto, and everyone involved in the real-world implementation.

#### REFERENCES

- [1] R. O'Reilly, J. Cohen, and J. Reichl, "Achievable load shifting potentials for the European residential sector from 2022–2050," *Renewable and Sustain. Energy Rev.*, vol. 189, 2024, Art. no. 113959.

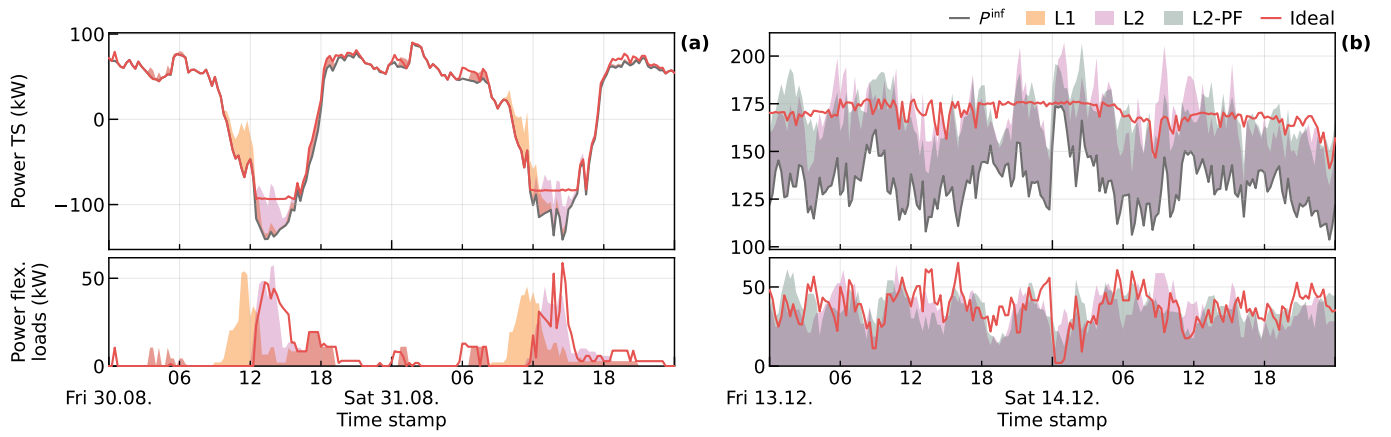


Fig. 6. Simulated TS load profiles for a selection of cases on two summer days (a) and two winter days (b).

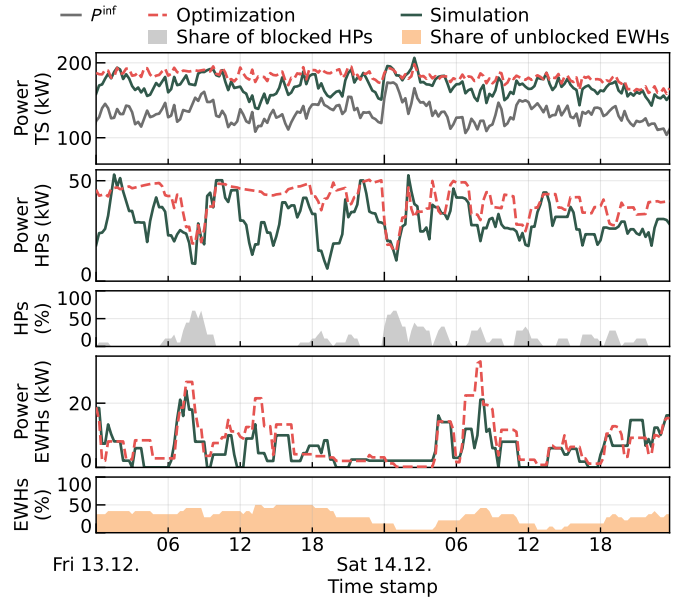


Fig. 7. Comparison between the optimization and simulation results for the formulation with perfect foresight, (L2-PF).

- [2] N. Damianakis, G. R. C. Mouli, and P. Bauer, "Grid impact of photovoltaics, electric vehicles and heat pumps on distribution grids — An overview," *Appl. Energy*, vol. 380, 2025, Art. no. 125000.
- [3] A. T. Procopiou and L. F. Ochoa, "Asset congestion and voltage management in large-scale MV-LV networks with solar PV," *IEEE Trans. Power Syst.*, vol. 36, no. 5, pp. 4018–4027, 2021.
- [4] International Energy Agency, "Unlocking the potential of distributed energy resources," Paris, 2022, Accessed: Jan. 6, 2026. [Online]. Available: <https://www.iea.org/reports/unlocking-the-potential-of-distributed-energy-resources>
- [5] D. S. Callaway and I. A. Hiskens, "Achieving controllability of electric loads," *Proc. of the IEEE*, vol. 99, no. 1, pp. 184–199, 2011.
- [6] E. Buechler, A. Goldin, and R. Rajagopal, "Improving the load flexibility of stratified electric water heaters: Design and experimental validation of MPC strategies," *IEEE Trans. Smart Grid*, vol. 15, no. 4, pp. 3613–3623, 2024.
- [7] Q. Cui, X. Wang, X. Wang, and Y. Zhang, "Residential appliances direct load control in real-time using cooperative game," *IEEE Trans. Power Syst.*, vol. 31, no. 1, pp. 226–233, 2016.
- [8] T. W. Ross and R. M. A. Smith, "Centralized ripple control on high-voltage networks," *J. of the Institution of Elect. Engineers - Part II: Power Eng.*, vol. 95, no. 47, 1948.
- [9] E. Ozkop, "A survey on direct load control technologies in the smart grid," *IEEE Access*, vol. 12, pp. 4997–5053, 2024.

- [10] E. Georges, B. Cornélusse, D. Ernst, V. Lemort, and S. Mathieu, "Residential heat pump as flexible load for direct control service with parametrized duration and rebound effect," *Appl. Energy*, vol. 187, pp. 140–153, Feb. 2017.
- [11] F. Ruelens, B. J. Claessens, P. Vranckx, F. Spiessens, and G. Deconinck, "Direct load control of thermostatically controlled loads based on sparse observations using deep reinforcement learning," *CSEE J. of Power and Energy Syst.*, vol. 5, no. 4, pp. 423–432, 2019.
- [12] K. R. Reddy and S. Meikandasivam, "Load flattening and voltage regulation using plug-in electric vehicle's storage capacity with vehicle prioritization using ANFIS," *IEEE Trans. Sustain. Energy*, vol. 11, no. 1, pp. 260–270, 2020.
- [13] N. Mahdavi, J. H. Braslavsky, M. M. Seron, and S. R. West, "Model predictive control of distributed air-conditioning loads to compensate fluctuations in solar power," *IEEE Trans. Smart Grid*, vol. 8, no. 6, pp. 3055–3065, 2017.
- [14] K.-Y. Huang and Y.-C. Huang, "Integrating direct load control with interruptible load management to provide instantaneous reserves for ancillary services," *IEEE Trans. Power Syst.*, vol. 19, no. 3, pp. 1626–1634, 2004.
- [15] F. Luo, J. Zhao, Z. Y. Dong, X. Tong, Y. Chen, H. Yang, and H. Zhang, "Optimal dispatch of air conditioner loads in Southern China region by direct load control," *IEEE Trans. Smart Grid*, vol. 7, no. 1, pp. 439–450, 2016.
- [16] C. Srithapon and D. Måansson, "Predictive control and coordination for energy community flexibility with electric vehicles, heat pumps and thermal energy storage," *Appl. Energy*, vol. 347, 2023, Art. no. 121500.
- [17] M. Starke, J. Munk, H. Zandi, T. Kuruganti, H. Buckberry, J. Hall, and J. Leverette, "Real-time MPC for residential building water heater systems to support the electric grid," in *2020 IEEE PES Innovative Smart Grid Technol. Conf. (ISGT)*, 2020.
- [18] E. Buechler, A. Goldin, and R. Rajagopal, "Designing model predictive control strategies for grid-interactive water heaters for load shifting applications," *Appl. Energy*, vol. 382, 2025, Art. no. 125149.
- [19] S. Xiang, L. Chang, B. Cao, Y. He, and C. Zhang, "A novel domestic electric water heater control method," *IEEE Trans. Smart Grid*, vol. 11, no. 4, pp. 3246–3256, 2020.
- [20] R. S. Tulabing, B. C. Mitchell, G. A. Covic, and J. T. Boys, "Localized demand control of flexible devices for peak load management," *IEEE Trans. Smart Grid*, vol. 14, no. 1, pp. 217–227, 2023.
- [21] M. Sullivan, J. Bode, B. Kellow, S. Woehleke, and J. Eto, "Using residential AC load control in grid operations: PG&E's ancillary service pilot," *IEEE Trans. Smart Grid*, vol. 4, no. 2, pp. 1162–1170, 2013.
- [22] F. Müller and B. Jansen, "Large-scale demonstration of precise demand response provided by residential heat pumps," *Appl. Energy*, vol. 239, pp. 836–845, 2019.
- [23] R. Gupta and J. Morey, "Evaluation of residential demand response trials with smart heat pumps and batteries and their effect at the substation feeder," *J. of Cleaner Prod.*, vol. 403, 2023, Art. no. 136760.
- [24] M. A. Adham, M. Obi, and R. B. Bass, "A field test of direct load control of water heaters and its implications for consumers," in *2022 IEEE Power & Energy Society General Meeting*, 2022.
- [25] Z. Zeng, D. Paresa, M. Adham, and R. B. Bass, "Field demonstration

of residential DER service-oriented load participation,” in *2024 IEEE Conf. on Technol. for Sustainability*, 2024, pp. 19–25.

[26] G. L. Aschidamini, M. Pavlovic, B. A. Reinholtz, M. S. Metcalfe, T. Niet, and M. Resener, “Comprehensive review on the control of heat pumps for energy flexibility in distribution networks,” *IEEE Access*, vol. 13, pp. 85 927–85 950, 2025.

[27] X. Cui, Y. Wang, and B. Xu, “Dimension-reduced optimization of multi-zone thermostatically controlled loads,” *IEEE Trans. Smart Grid*, vol. 16, no. 6, pp. 4685–4697, 2025.

[28] B. Knueven, J. Ostrowski, and J.-P. Watson, “On mixed-integer programming formulations for the unit commitment problem,” *INFORMS J. on Comput.*, vol. 32, no. 4, pp. 857–876, 2020.

[29] M. Kreft, T. Brudermueller, T. Anderson, and T. Staake, “Identifying electric water heaters from low-resolution smart meter data,” in *2024 IEEE Conf. on Technol. for Sustainability*, 2024, pp. 128–135.

[30] K. Kaiser, M. Kreft, M. Guscetti, G. Valverde, L. Leenders, M. González Vayá, T. Staake, and G. Hug, “OrtsNetz,” Bern, 2025, Accessed: Aug. 13, 2025. [Online]. Available: <https://www.aramis.admin.ch/Default?DocumentID=73403>

[31] Gurobi Optimization, LLC, “Gurobi Optimizer Reference Manual,” 2023. [Online]. Available: <https://www.gurobi.com>

[32] K. Kaiser, M. Kreft, and G. Hug, “Peak reduction via time-variable tariffs and automated load control: Results from a Swiss pilot study,” 2025, Accessed: Nov. 6, 2025. [Online]. Available: <http://dx.doi.org/10.2139/ssrn.5705205>

[33] K. Kaiser and G. Hug, “Dynamic grid tariffs for power peak reduction using reinforcement learning,” in *2024 Int. Conf. on Smart Energy Syst. and Technol. (SEST)*, 2024.

[34] A. Heider, L. Kundert, B. Schachler, and G. Hug, “Grid reinforcement costs with increasing penetrations of distributed energy resources,” in *2023 IEEE Belgrade PowerTech*, 2023.